Available online at
https://journal.uitm.edu.my/ojs/index.php/MJCET

e-ISSN: 2682-8588

Malaysian Journal of Chemical Engineering & Technology 7(2) 2024, 49–61

Malaysian Journal of Chemical Engineering and Technology

A novel combined-mode design for a MEMS-based micro passive direct methanol fuel cell

Umi Azmah Hasran[1*], Siti Kartom Kamarudin[2], Burhanuddin Yeop Majlis[3], Gandi Sugandi[4]

[1,2] *Fuel Cell Institute, Universiti Kebangsaan Malaysia, 43600 Bangi, Selangor, Malaysia*
[3] *Institute of Microengineering and Nanoelectronics, Universiti Kebangsaan Malaysia, 43600 Bangi, Selangor, Malaysia*
[4] *Research Center for Electronics, National Research and Innovation Agency, Bandung 40135, West Java, Indonesia*

ARTICLE INFO

Article history:
Received 31 March 2024
Revised 8 August 2024
Accepted 11 August 2024
Online first
Published 31 October 2024

Keywords:
Flow field
MEMS
Fuel cell applications
Micromachining
Electrode plate
Modelling

DOI:
10.24191/mjcet.v7i2.1295

ABSTRACT

A small-scale micro direct methanol fuel cell was developed by utilizing silicon substrate-based electrode plates, where the flow field plate was fabricated with micro-electro-mechanical system technology. Modelling work was carried out to assist in designing the anode and cathode plates to obtain the required configuration and geometric dimensions for the microfabrication process. A novel combined-mode anode plate was developed with an active-mode grid design and a passive-mode porous design for the flow field while the cathode plate was developed with a passive-mode design of square window-shaped through holes in a staggered arrangement. Silicon etching methods were used to form the desired flow field structures on the electrode plates with an active area of 1 cm^2. The single cell was assembled by incorporating the electrode plates and membrane electrode assembly. A study on the feasibility and effectiveness of the new micro fuel cell was conducted. The performance test resulted in a maximum power density value of 1.86 mW/cm^2 at a voltage of 138.7 mV.

1. INTRODUCTION

As a developing country, Malaysia displays high carbon emissions and is currently working towards transitioning to cleaner energy sources. Greenhouse gases emissions have been widely acknowledged as the primary cause of global warming, leading to climate change and environmental impacts worldwide (Kamarudin et al., 2022; Kandar et al., 2023). In recent years, fuel cells have garnered substantial attention as promising energy sources, particularly in replacing traditional battery technology for mobile devices due to their potential for higher energy density. The direct methanol fuel cell (DMFC) emerges as a standout power source for mobile applications, offering advantages such as high energy density and safer handling, given that methanol fuel exists in liquid form under ambient conditions. This liquid fuel eliminates the need

[1*]Corresponding author. *E-mail address*: umi.h@ukm.edu.my
https://doi.org/10.24191/mjcet.v7i2.1295

for complex reforming systems and a large balance of plant (BOP), thereby simplifying system design (Jayakumar et al., 2021). This power output distinction delineates the boundary between micro and mini fuel cells, showcasing their versatility in addressing diverse power requirements. Essential fuel cell components include anode and cathode plates, membrane electrode assembly (MEA), proton exchange membrane, catalyst layer, gas diffusion layer, and current collector layer (Luo et al., 2021).

Despite substantial progress in fuel cell technology, the downscaling of electrode plate size using silicon (Si) substrates for micro fuel cells through microfabrication based on micro-electro-mechanical systems (MEMS) technology presents challenges necessitating meticulous planning, characterisation, and specialised microfabrication processes. The flow channel referred to as the flow field, and the flow plate, generally known as the separator plate or electrode plate, play pivotal roles in ensuring the uniform distribution of reactants and effective removal of byproducts from the fuel cell. While previous works provide insights into conventional fuel cell components (Barbera & Giacoppo, 2020), a notable research gap exists in microfabrication techniques specific to micro direct methanol fuel cells (µDMFCs) (Alias et al., 2020; Fadzillah et al., 2019; Ismail et al., 2019). The microfabrication process involves etching Si wafers to create the intricate structure of the electrode plate. Although wet etching with potassium hydroxide (KOH) solution remains a sustainable and conventional choice in MEMS techniques, laser ablation emerges as a versatile alternative overcoming limitations related to etch selectivity and orientation of the silicon crystal plane (Wang & Yang, 2021). Laser ablation, not requiring photolithography, enables the production of complex Si structures with various shapes and contours, providing a more flexible design approach.

In this context, the proposed research aims to address the existing research gap by developing a novel flow field structure in the electrode plate of a µDMFC. The novelty lies in combining designs serving different distribution functions on the electrode plate, with a specific emphasis on the anode plate's flow field design. This research is critical as efficient fuel transport significantly influences the overall performance of micro fuel cells. This work contributes to the ongoing efforts to enhance micro fuel cells' performance and practical viability, ultimately paving the way for their broader adoption in various applications.

2. MATERIALS AND METHODS

The research encompasses five (5) key steps. Step 1 focuses on the design and modelling aspects of the flow fields. Step 2 involves the development and characterisation of microfabrication processes that leverage mems technology. This facet aims to enhance the understanding and application of intricate fabrication techniques. Step 3 investigates the manufacturing and optimisation aspects, employing the design of experiments (doe) method to ensure efficiency and precision in the production processes. Step 4 centres on the crucial phase of integration, where all individual components were harmoniously brought together for comprehensive development and assembly. Finally, step 5 entails the testing of DMFC performance by assessing the functionality and durability of the assembled fuel cell. Together, these steps form a comprehensive strategy to advance the understanding, development, and implementation of microfabrication processes for the specified application.

2.1 Design and modelling

The µDMFC in this study incorporated the microfabricated anode and cathode silicon plates in its assembly. The novel anode electrode structure introduced a combined-mode µDMFC for the anode plate by integrating two distinct flow field designs: the grid flow field (active mode) and the porous flow field (passive mode). The anode flow field had a structure of four square-shaped platforms, which constitute the

https://doi.org/10.24191/mjcet.v7i2.1295

grid flow field design. The characteristics and dimensions of the anode plate with the new flow field design concept were determined by considering several limiting factors:

(i) The open area ratio was at ~ 50% for a 1 cm^2 active electrode area

(ii) The dimensions of the capillaries were determined by sufficient capillary pressure

(iii) The flow inside the cross-flow channel was laminar

(iv) The dimensions of the inlet/outlet channels were determined by the fuel tube size.

(v) The number of capillaries on one rib was limited by the length of the grid side

The microfabrication process to form the required electrode structure utilised a laser ablation process, which is a bulk micromachining technique without photoresist that does not depend on etch selectivity and Si plane orientation, to form the desired plate structure. The geometric dimensions for the anode and cathode plates are shown in Fig. 1 and detailed in Table 1 and Table 2, respectively. The origin point (0,0) coordinates were established at the bottom-left corner of the silicon plate, serving as the starting point for each laser ablation process to create structures on the plate. The same sized plate area, *L*, and reaction active area, *V*, were used for both plates in the microfabrication process, i.e., 25 mm × 25 mm and 10 mm × 10 mm, respectively. The process involved etching 13 and 14 contact areas for the anode plate and cathode plate, respectively.

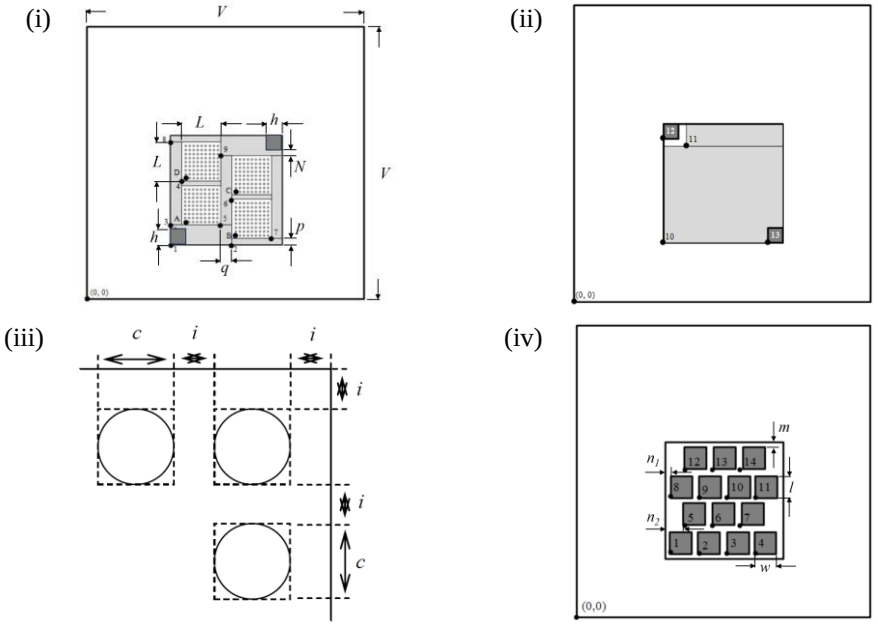

Fig. 1. Schematics of flow fields for the (i) platform structure of the grid design in the anode plate, (ii) fuel reservoir structure on the anode side, (iii) porous capillary structure within the grid area, and (iv) square window-shaped through holes design in the cathode plate in a staggered arrangement

Source: Authors' own data

https://doi.org/10.24191/mjcet.v7i2.1295

Table 1. Geometric dimension settings of the anode plate

Parameter	Value
Side length of through hole, *h*	1.7 mm × 1.7 mm
Distance between through hole and platform edges, *N*	0.883 mm
A, B, C, and D grid platform area, *L*	3.31 mm × 3.31 mm
Channel width, *p*	0.492 mm
Channel width, *q*	1.13 mm
Methanol reservoir depth	300 mm
Channel depth = grid platform height	100 mm
Distance between capillaries, *i*	0.1 mm
Capillary diameter, *c*	0.1 mm
Opening area ratio	56%

Source: Authors' own data

Table 2. Geometric dimension settings of the cathode plate

Parameter	Value
Reaction active area	10 mm × 10 mm
Side length of through hole (*l*, *w*)	1.85 mm × 1.85 mm
Distance *m*, n_1	0.52 mm
Distance n_2	1.705 mm
Silicon wafer thickness	1.108 mm
Opening area ratio	48%

Source: Authors' own data

Modelling work was conducted through computational fluid dynamics (CFD) by utilising the COMSOL Multiphysics software to ascertain the flow field designs for the anode plate. The grid flow field simulation aimed to finalise the fabrication configuration, while the simulation for the porous flow field focused on verifying the grid flow field arrangements and the dimensions of the capillary structure. In three-dimensional (3D), the subdomain was partitioned into tetrahedral elements by the mesh generator. The model encompassed a total of 52,853 degrees of freedom, and the resultant mesh comprised 7,829 tetrahedral elements. The minimum overall element quality was determined as 0.2541. The flow geometry within the grid flow field was resolved utilizing the UMFPACK direct linear system solver, recognised as the default solver for linear systems in most application modes. The governing equations for this model were summarised based on the following assumptions:

(i) Constant physical properties

(ii) Newtonian fluid with constant viscosity

(iii) Isothermal conditions

(iv) Steady-state flow

Fluid flow was assumed to be at a steady state and with a uniform distribution. The incompressible Navier-Stokes application mode and the no-slip boundary condition were used for the fluid flowing in the

https://doi.org/10.24191/mjcet.v7i2.1295

flow field and the inlet/outlet of the channel. The velocity vector was oriented perpendicular to the boundary, with the velocity component in the y-direction set to 0.01 m/s at the inlet boundary, and the velocity component in the x-direction was set to zero.

2.2 Microfabrication Process

Silicon (Si) wafer is a semiconductor material and requires a metal layer that can act as a current collector to reduce the ohmic resistance and promote the flow of electricity in the micro fuel cell. The microfabrication of the silicon substrate was carried out with careful consideration of the limitations and operational requirements during the design and modelling step to ensure the optimal distribution of reactants and removal of by-products in the anode and cathode channels of the µDMFC. Laser ablation facilitated flow field etching of the anode plate, enabling its use in the active–passive mode of the µDMFC. The Si wafer used to produce the electrode plate was a p-type <100> substrate with a diameter of 4 inches, a thickness of 500 ± 20 µm, and a resistance of 0–20 Ω·cm. Limitations in the microfabrication process and micro fuel cell operation requirements were considered to ensure good distribution of reactants and removal of byproducts in the anode and cathode channels. A thin layer of silicon dioxide (SiO_2) was used as a protective mask during the laser ablation process. The SiO_2 layer was grown using a method for the thermal oxidation process (Hasran et al., 2011) to a thickness of up to 2 µm at high temperature (800–1100 °C) in an oxygen-rich environment. The SiO_2 layer worked to protect the Si surface from severe damage during the annealing process. This layer also provided hydrophilic properties to the capillary walls to reduce capillary pressure drop and acted as an electrical insulating layer between the current collector metal layer and the Si substrate.

The laser system used was GSI Lumonics W670 Laser Trim (General Scanning Inc., Somerville, US), with Neodymium (Nd: Y3Al5O12). The laser scan speed could be controlled with mirrors and the ablation process became very fast to enable high throughput processing. The laser operation in this work required only electricity, and this is different from other laser operations that require additional chemicals during processing. The sample also did not need to be handled by hand during processing, and this reduced the risk of contamination. The wafer was cut to a size of 25 mm × 25 mm using a laser beam to produce the sample. For the anode plate, the grid flow field consisted of square-shaped platforms in a shallow groove, which also acted as channels, facilitating the transport of fuel and by-products via a liquid pump. The porous flow field within each grid platform featured a capillary array that propelled fuel toward the active reaction site, as shown in Fig. 2.

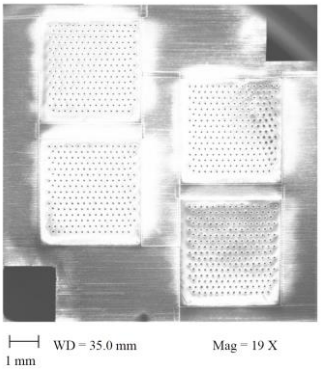

Fig. 2. Capillary arrays were created through laser ablation for four platforms in the grid flow field of the anode plate

Source: Authors' own data

https://doi.org/10.24191/mjcet.v7i2.1295

For the cathode plate, the laser program produced a square-shaped through-holes flow field array (Hasran et al., 2019a; Hasran et al., 2019b). This design aimed to achieve a 50% utilisation of the MEA active area for the micro fuel cell. Current collectors, deposited through the sputtering of conductive metals onto the wafer surface, effectively mitigated ohmic resistance in the micro fuel cell.

2.3 Manufacturing and optimisation

In this step, the MEA was manufactured using parameters optimised by a method for its hot-pressing process. The MEA consisted of a Nafion 117 membrane and porous electrodes, each with a 1 cm^2 active area. The Pt and Pt/Ru catalysts were loaded at 8 $mg \cdot cm^{-2}$ for the cathode and anode sides, respectively. The cathode and anode electrodes were aligned on both sides of the membrane and hot-pressed. The optimised parameters were obtained with response surface methodology (RSM) and central composite design (CCD) using a statistical software package, Design-Expert (Hasran et al., 2013).

2.4 Development and assembly

The optimised MEA was pre-treated by immersing it in deionised water (DIW) at 80 °C for 2 hours. The contact surface of the silicon plates was coated with the conductive gold (Au) layer, serving as a current collector to facilitate electricity conduction within the cell. The microfabricated anode and cathode plates were subsequently integrated with the MEA to form a single cell, as shown in Fig. 3. The cathode side was exposed to ambient air, while the anode side incorporated a built-in reservoir structure on the back of the anode plate that matched the reaction active area and thereby provided additional fuel storage capacity.

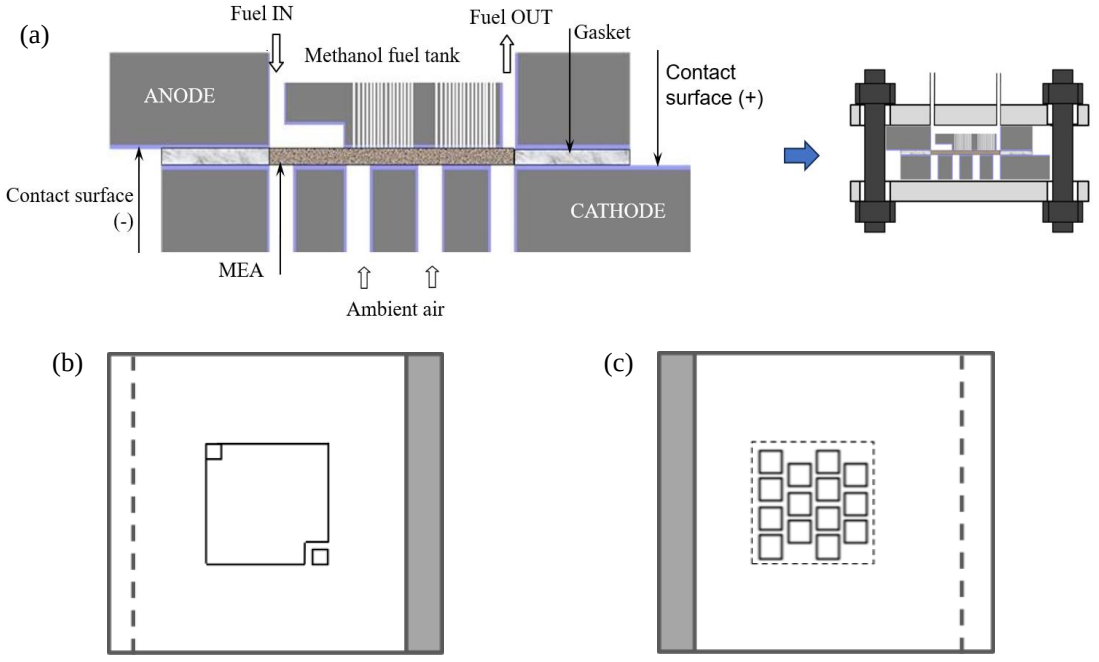

Fig. 3. Schematic of the (a) cross-section view of the micro DMFC assembly with (b) top and (c) bottom views

Source: Authors' own data

https://doi.org/10.24191/mjcet.v7i2.1295

2.5 Performance testing

Performance testing was conducted to obtain polarisation and power density curves under ambient conditions. The tests were done using the Potentiostat/Galvanostat model WMPG1000. This WMPG1000 system had a voltage range of ± 20 V and a current range of 5 A, 50 mA, and 500 µA. The methanol fuel was supplied to the cell at a flow rate of 2 mL/min, facilitated by a Manostat Compulab 3 peristaltic pump.

3. RESULTS AND DISCUSSIONS

The inlet/outlet and flow field channels played a crucial role in ensuring continuous fuel flow for active mode operation within the cell, making their study essential for analysing the anode plate design. The visualisation and measurement study undertaken via modelling and simulation of the flow fields examined the configuration effects of different inlet/outlet arrangements on fuel flow characteristics inside the µDMFC. There were two configurations investigated for the anode flow field design. Fig. 4(a) shows the grid platforms are arranged in straight rows with both inlet/outlet holes located at the end edges of the flow field, while Fig. 4(b) shows the grid platforms are arranged in a staggered pattern with inlet/outlet holes positioned opposite each other. Furthermore, the magnification of a cross-sectional cut of the grid platform structure for the flow field demonstrates the symmetrical geometric areas within the capillary structure that will be simulated. The symmetrical cross-sectional geometry illustrated in Fig. 4(c) was employed for simulating two-phase flow for the vertical capillary column above the reservoir containing a methanol fuel-equivalent fluid in the model.

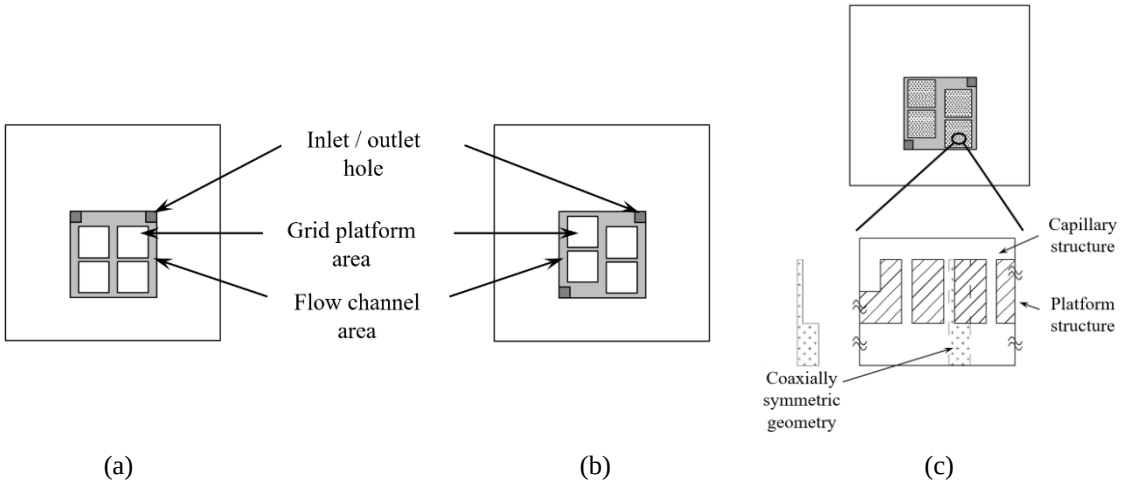

Fig. 4. Anode flow field configurations for simulation: (a) grid platforms in a straight arrangement, (b) grid platforms in a staggered arrangement, and (c) enlarged view of the grid platform showing a cross-sectional image illustrating the symmetrical geometric areas for capillary structure

Source: Authors' own data

In this model, the outlet boundary pressure was set at the atmospheric value of 1.013 kPa. The results shown in Fig. 5(a) and (b) indicated that the maximum pressure for the staggered flow field was approximately 1.023 kPa, contrasting with the maximum pressure of around 1.029 kPa for the flow field in a straight arrangement. This resulted in a higher pressure drop of nearly 60% between the inlet and outlet

https://doi.org/10.24191/mjcet.v7i2.1295

for the staggered flow field and the flow velocity can be seen to increase with increasing pressure difference. From this result, the flow velocity can be expected to increase with the rising pressure difference, thereby enhancing methanol transport efficiency.

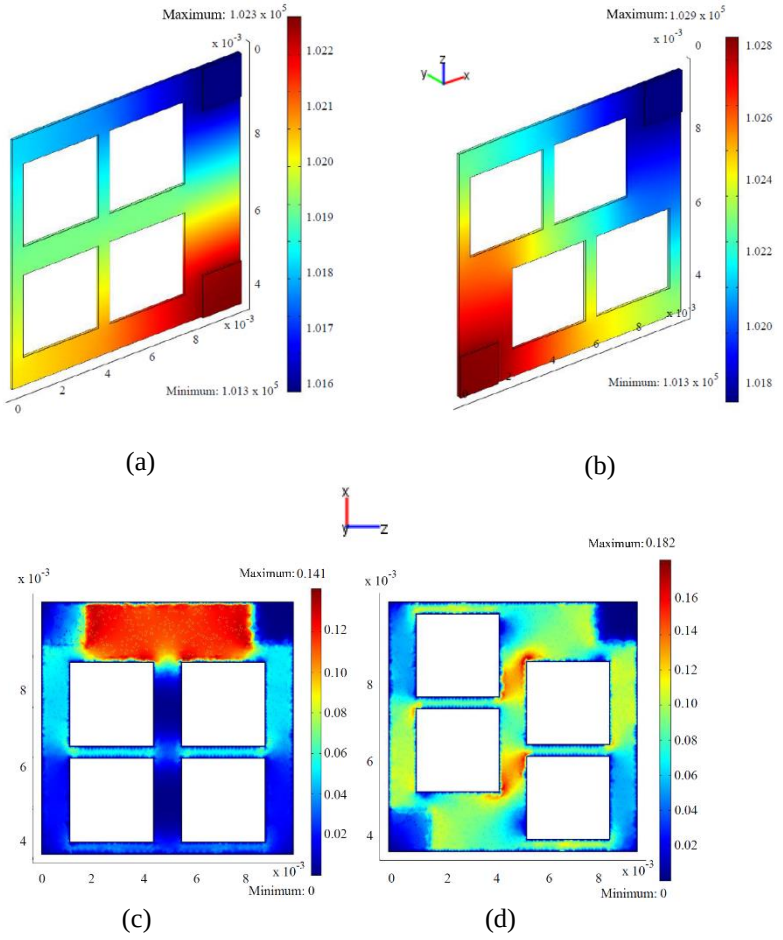

Fig. 5. The illustration shows the pressure distribution for the (a) straight versus (b) staggered flow field arrangements and the magnitude of flow velocity in a channel for the (a) straight versus (b) staggered flow field arrangements

Source: Authors' own data

Fig. 5(c) and (d) compares the distribution of fuel convection velocity between the two studied systems, revealing the impact of inlet/outlet position on flow distribution. Velocity magnitudes depicted by blue to red contours represented weak to high flows, respectively. In a vertically oriented model with the inlet at the bottom, fuel flowed through the channel surrounding the platform structures against the force of gravity and out through the outlet hole at the top of the flow field. For the straight arrangement, the positions of the inlet/outlet channels directed the fuel flow to prioritise paths with less resistance, which were farther from the channel areas around the grid plate. This resulted in high flow velocities in the regions between the inlet/outlet channels but significantly lower and almost stagnant flow in the central region of the flow field.

https://doi.org/10.24191/mjcet.v7i2.1295

For the staggered arrangement, fuel gradually moved from the inlet to the outlet with a more uniform velocity magnitude, and the high-velocity flow areas were concentrated in the middle part of the flow field. This suggested that the staggered flow field promotes a more even fuel distribution in the cell.

Capillarity is the tendency of fluids to rise in capillary columns (Urone et al., 2012). Cohesive forces between molecules in the fuel cause the liquid surface to contract to minimise surface area, resulting in surface tension, a crucial parameter in capillary effect studies. F_{st} in Fig. 6 refers to the force of surface tension. Fluid adhesion to the walls exerts an upward force on the liquid edges, creating a concave meniscus, while surface tension acts to maintain the integrity of the surface, causing both the liquid edges and the entire liquid surface to be pulled upward. Capillarity can move the fuel horizontally over great distances, but the vertical distance it can move the fuel is limited by the weight of the fuel in the column. The choice of capillary centreline also greatly influences parameters such as pressure, flow rate, and fuel rise. The pressure for the liquid in the capillary column (P_1) was lower than the pressure for the gas at atmospheric pressure (P_0). The pressure difference between the meniscus surfaces in the column creates capillary pressure and causes the fuel to rise in the capillary column. The dashed line illustrates the shape of the liquid if it did not experience the effect of surface tension attempting to flatten it. The contact angle, θ, emerges at the contact line between three different phases: air (gas)-fuel (liquid)-capillary wall (solid) and is an important parameter as it is directly related to the curvature radius between the gas-liquid interface and the surface tension between different phases. The relative strength of cohesive and adhesive forces affects θ, where if the cohesive force is greater relative to the adhesive force, the value of θ is also larger and the liquid surface tends towards a convex shape. Conversely, if the adhesive force is greater relative to the cohesive force, the value of θ becomes smaller and the adhesive force can flatten the meniscus. The fuel is drawn upwards if $\theta < 90°$ and its rise is inhibited if $\theta > 90°$. This simulation assumed that perfect wetting occurred for the methanol fuel (aqueous solution), which is an organic liquid, i.e., $\theta = 0$. The capillary forces were solved using the Young-Laplace equation (shown in Eq. (1) from the classical two-phase model.

$$F_{rise} = \sigma_{mix} \cdot (2\pi r) \cdot \cos\theta \quad (1)$$

where σ_{mix} is the surface tension coefficient of the fuel (N/m), $2\pi r$ is the perimeter of the capillary with a circular shape, and θ is the contact angle between the solid surface, namely the capillary wall, and the liquid, namely the fuel. The corresponding pressure due to capillary action is as Eq. (2):

$$P = F_{rise} / \pi r^2 \quad (2)$$

The surface tension value was also used to determine the height of the fuel column, h, required for sufficient capillary pressure for the fuel to rise due to capillary action from the reservoir to reaction area (Eq. (3):

$$h = 2.\sigma_{mix} \cdot \cos\theta / rg\rho_{mix} \quad (3)$$

where ρ is density (kg/m^3), r is capillary radius (m), and g is gravity constant.

A two-dimensional (2D) capillary flow model was developed to depict fluid flow within the capillary structure located in the grid design. Two-phase fluid motion (gas, i.e., air, and liquid, i.e., methanol fuel) was resolved using the level set method. The degree of freedom (DOF) for this model was 43304, and the final mesh consists of only quadrilateral elements, namely 3250, with an overall minimum element quality of 0.80. Capillary geometry was solved using the direct linear solver system parameterised PARDISO. Fig. 6 illustrates the impact of pressure on the ascent of fuel in the capillary at various methanol concentrations within the considered range of capillary diameters for this simulation.

https://doi.org/10.24191/mjcet.v7i2.1295

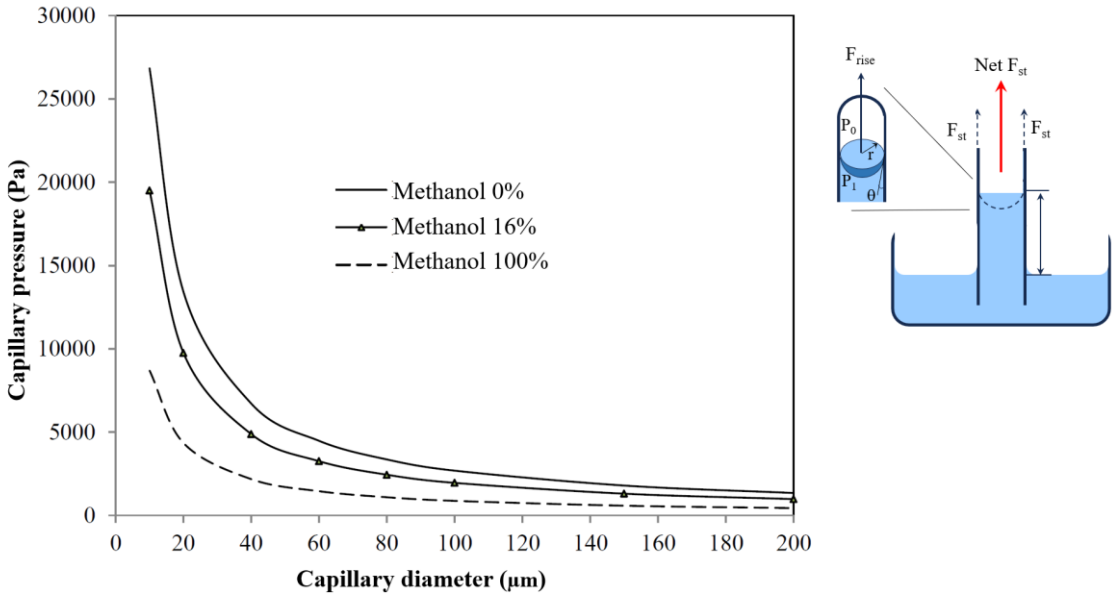

Fig. 6. Simulated pressure curve at different methanol concentrations and capillary diameters

Source: Author's own data

The methanol curve represents pure methanol (100% concentration), and the pure water curve represents 0% methanol concentration, establishing the boundaries for the concentration of methanol used as fuel in this simulation, set at 16%w/w (or 5 M). While the graph displays a consistent trend of decreasing pressure with increasing capillary diameter and methanol concentration within the fuel, a shallow slope was evident in the diameter range of 60 to 200 µm. This indicates that, in this range, the impact of diameter on capillary pressure is almost negligible. The pressure gradient propelled the fuel upward, ensuring continuous ascent until it reached the top of the column and reached the active area on the anode electrode for the electrochemical reaction. Therefore, the limiting factor for capillary action is the diameter of the capillary, which, in turn, is limited by the microfabrication process.

Based on these results, the electrode plates were microfabricated and assembled with the optimised MEA to form the µDMFC. The performance test was carried out to study the workability of the new anode design at different cell orientations, as shown in Fig. 7. Before running each performance test, the MEA was activated by flowing methanol fuel without current load, or open-circuit voltage (OCV), to obtain credible data in stable operating conditions. The stability of the output voltage was observed at a slow methanol flow rate of 2 mL/min while the methanol solution concentration was maintained at 5 M. All cell performance tests were conducted under the same operating conditions and at room temperature (~30 °C).

A comparison of cell performance curves in the horizontal and vertical orientation was plotted for the open circuit voltage (OCV) and I-V values as shown in Fig. 8(a) and (b), respectively. The cell voltage curve increased to a point where it levelled off and the test was stopped when the curve started to decrease to prevent cell performance from deteriorating severely. For the same cell design and methanol concentration, the OCV value during stable operation also indicates that the vertical cell performed better under no-load current conditions. A better performance was obtained at low and high current densities for

https://doi.org/10.24191/mjcet.v7i2.1295

the vertically oriented cell with a maximum power of 1.86 mW·cm^{-2} at a voltage of 138.7 mV. This is probably due to the CO_2 and water removal being aided by the gravitational force of the vertical cell. Meanwhile, CO_2 bubbles are more likely to occupy any open areas within the channels across the reaction surface in the horizontal cell, adding hindrance to the reaction area and increasing mass transport resistance.

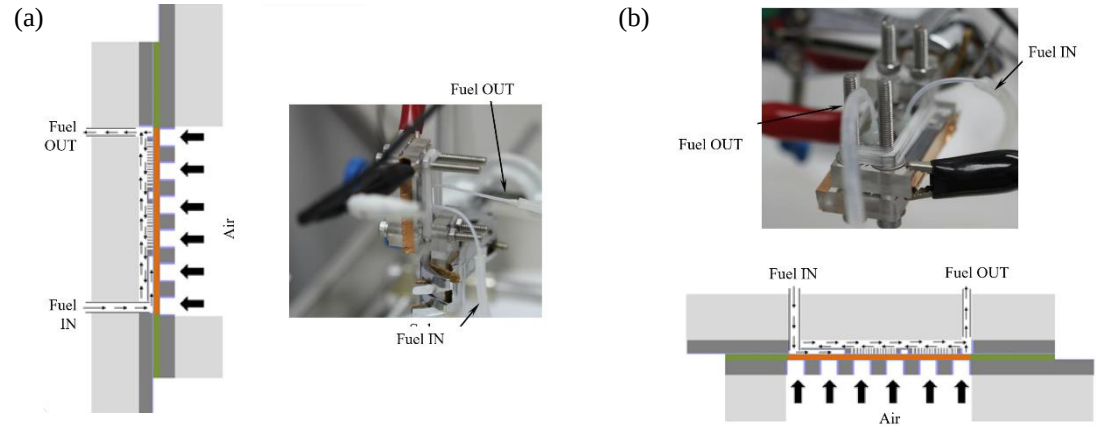

Fig. 7. Schematic diagrams and photos of the assembled µDMFC in: (a) vertical orientation and (b) horizontal orientation

Source: Authors' own data

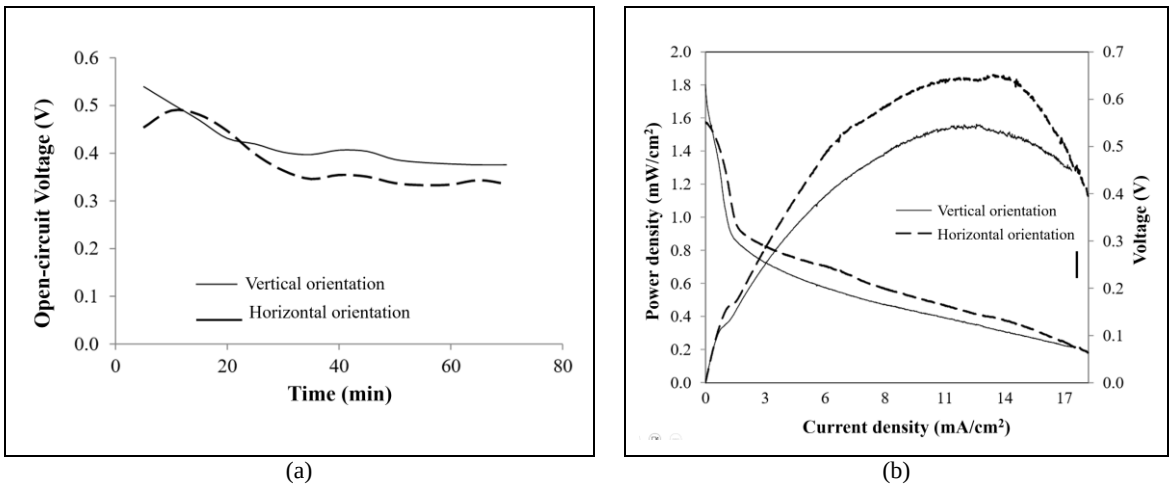

(a) (b)

Fig. 8. Characterisation curves at different cell orientations for: (a) open circuit voltage and (b) cell performance

Source: Authors' own data

https://doi.org/10.24191/mjcet.v7i2.1295

4. CONCLUSIONS

A micro direct methanol fuel cell was assembled consisting of silicon substrate-based electrode flow field plates microfabricated using micro-electro-mechanical system (MEMS) technology. Modelling guided the design of the anode and cathode plates, ensuring optimal configuration and dimensions for microfabrication. A laser ablation process was utilised to form intricate flow field structures on the electrode plates. The novel combined-mode anode plate design and staggered square window-shaped through holes design for the cathode plate with an active area of 1 cm^2 of MEA yielded promising results. Performance testing showcased a maximum power density of 1.86 mW/cm^2 at 138.7 mV, affirming the potential of this micro fuel cell technology for mobile applications.

ACKNOWLEDGEMENTS AND FUNDING

The authors gratefully acknowledge the financial support the Ministry of Higher Education of Malaysia provided under the program HICOE-2023-008. Additionally, this research received funding from Universiti Kebangsaan Malaysia through TAP-K014919 and the Ministry of Higher Education of Malaysia under research codes UKM-TR2022-11 and FRGS/1/2016/TK09/UKM/03/1.

CONFLICT OF INTEREST STATEMENT

The authors agree that this research was conducted in the absence of any self-benefits, commercial or financial conflicts and declare the absence of conflicting interests with the funders.

AUTHORS CONTRIBUTIONS

Umi Azmah Hasran: Conceptualisation, methodology, investigation, visualisation, validation, formal analysis, and writing-original draft; **Siti Kartom Kamarudin**: Project administration, funding acquisition, resources, supervision, and writing-review & editing; **Burhanuddin Yeop Majlis**: Resources and supervision; **Gandi Sugandi**: Conceptualisation, methodology, and software.

REFERENCES

Alias, M. S., Kamarudin, S. K., Zainoodin, A. M., & Masdar, M. S. (2020, 2020/07/31/). Active direct methanol fuel cell: An overview. *International Journal of Hydrogen Energy, 45*(38), 19620–19641. https://doi.org/https://doi.org/10.1016/j.ijhydene.2020.04.202

Barbera, O., & Giacoppo, G. (2020). 12 - Stack and bipolar plates design for direct methanol fuel cells. In K. Dutta (Ed.), *Direct methanol fuel cell technology* (pp. 341–376). Elsevier. https://doi.org/https://doi.org/10.1016/B978-0-12-819158-3.00012-4

Fadzillah, D. M., Kamarudin, S. K., Zainoodin, M. A., & Masdar, M. S. (2019). Critical challenges in the system development of direct alcohol fuel cells as portable power supplies: An overview. *International Journal of Hydrogen Energy, 44*(5), 3031–3054. https://doi.org/https://doi.org/10.1016/j.ijhydene.2018.11.089

Hasran, U. A., Kamarudin, S. K., Daud, W. R. W., Majlis, B. Y., Mohamad, A. B., & Kadhum, A. A. H. (2011). A simple thermal oxidation technique and KOH wet etching process for fuel cell flow field fabrication. *International Journal of Hydrogen Energy, 36*(8), 5136–5142. https://doi.org/https://doi.org/10.1016/j.ijhydene.2011.01.043

https://doi.org/10.24191/mjcet.v7i2.1295

Hasran, U. A., Kamarudin, S. K., Daud, W. R. W., Majlis, B. Y., Mohamad, A. B., Kadhum, A. A. H., & Ahmad, M. M. (2013). Optimization of hot-pressing parameters in membrane electrode assembly fabrication by response surface method. *International Journal of Hydrogen Energy, 38*(22), 9484–9493. https://doi.org/https://doi.org/10.1016/j.ijhydene.2012.12.054

Hasran, U. A., Kamarudin, S. K., Majlis, B. Y., Daud, W. R. W., Kadhum, A. A. H., & Sugandi, G. (2019a). Laser-assisted silicon etching for micro fuel cell electrode plate fabrication. *Malaysian Journal of Analytical Science, 23*(2), 345–354. https://doi.org/ https://doi.org/10.17576/mjas-2019-2302-18

Hasran, U. A., Kamarudin, S. K., Majlis, B. Y., Ramli, W. K. W., Daud, W. R. W., & Kadhum, A. H. (2019b). Nd:YAG laser fabrication of silicon electrode plates for a combined-mode micro direct methanol fuel cell. *Malaysian Journal of Analytical Sciences, 23*(2), 362–375. https://doi.org/10.17576/mjas-2019-2302-20

Ismail, A., Kamarudin, S. K., Daud, W. R. W., Masdar, S., & Hasran, U. A. (2019). Development of optimisation model for direct methanol fuel cells via cell integrated network. *International Journal of Hydrogen Energy, 44*(58), 30606–30617. https://doi.org/https://doi.org/10.1016/j.ijhydene.2019.05.209

Jayakumar, A., Madheswaran, D. K., & Kumar, N. M. (2021). A critical assessment on functional attributes and degradation mechanism of membrane electrode assembly components in direct methanol fuel cells. *Sustainability, 13*(24), 13938. https://doi.org/10.3390/su132413938

Kamarudin, N., Sinniah, G. K., & Mohamad Husny Hamid, Z. J. (2022). Managing transportation challenges in selected Southeast Asia countries: Comparison of policies, framework, and components. *Malaysian Journal of Sustainable Environment, 9*(3) Special Issue, 41–59 https://doi.org/10.24191/myse.v9i3.18290

Kandar, M. Z., Muszaffarsham, N. H., Mohd Husini, E., Md Norwawi, N., & Khairi, K. F. (2023). Enhancing energy efficiency through the incorporation of Maqasid Syariah knowledge: A Review. *Malaysian Journal of Sustainable Environment; Vol 10 No 1 (2023): MySE.Vol.10.No.1*. https://doi.org/10.24191/myse.v10i1.21256

Luo, Y., Wu, Y., Li, B., Mo, T., Li, Y., Feng, S.-P., Qu, J., & Chu, P. K. (2021, 2021/10/01/). Development and application of fuel cells in the automobile industry. *Journal of Energy Storage, 42*, 103124. https://doi.org/https://doi.org/10.1016/j.est.2021.103124

Urone, P. P., Hinrichs, R., Dirks, K., Sharma, M., Podolak, K., & Smith, H. (2012). *College Physics*. OpenStax https://openstax.org/details/books/college-physics-2e

Wang, H.-J., & Yang, T. (2021, 2021/08/01/). A review on laser drilling and cutting of silicon. *Journal of the European Ceramic Society, 41*(10), 4997–5015. https://doi.org/https://doi.org/10.1016/j.jeurceramsoc.2021.04.019

https://doi.org/10.24191/mjcet.v7i2.1295